Journal of Asian Concrete Federation
Vol. 11, No. 2, pp. 69-80, June 2025
ISSN 2465-7964/ eISSN 2465-7972
DOI http://dx.doi.org/10.18702/acf.2025.11.2.69

Technical Paper

Effect of nanosilica and silica fume on supersulfated cement properties and hydration

Tongzhou Cai, Kim Hung Mo*, Heng Chen, Pengkun Hou*

(Received: 14-Apr-2025; Revised: 06-Jun-2025; Accepted: 09-Jun-2025; Published online: 25-Jun-2025)

Abstract: The article provides a comparative analysis of the hydration effects of nanosilica (NS) and silica fume (SF) in supersulfated cement, investigating the reasons for the differences between their effects. The effects of the addition of 3% NS and SF on the macroscopic and microscopic properties of supersulfated cement were studied. The experimental results show that the compressive strength of NS group is lower than that of SF group in low-clinker samples, while in high-clinker samples, presenting an opposite trend, and NS and SF can sustainably increase the compressive strength, and the long-term effect is more evident. In addition, both NS and SF can reduce the hydration heat due to hindering the formation of ettringite, and the inhibitory effect of NS is greater than that of SF. Moreover, NS will significantly decrease the pH value and saturation index, and drastically reduce the concentration of calcium ion, while SF has no obvious effect on this. This study highlights that NS is more suitable for high-clinker SSC systems (e.g., structural engineering requiring long-term strength), while SF performs better in low-clinker systems (e.g., eco-friendly pavements), providing a theoretical basis for material selection in practical engineering.

Keywords: Nanosilica, Silica fume, Compressive strength, pH, calcium ion.

1. Introduction

The cement industry is a significant contributor to carbon emissions, accounting for approximately 8% of the total carbon emissions worldwide[1]. With the continued rise in global carbon dioxide concentration, it is crucial to reduce the carbon emissions of the cement industry. supersulfated cement (SSC) is a typical low-carbon cement[2], therefore, the development and application of SSC is one of the effective way to reduce carbon emissions in the cement industry and alleviate ecological pressure.

SSC is a type of cement composed of 75-85 wt % slag, 10-15 wt% sulfate (such as gypsum or phosphogypsum[3]), and 1-5 wt% alkaline activator[4] (typically clinker or portland cement). The alkaline activator mainly provides the calcium ion needed for the chemical reaction. During the hydration process of SSC, the main hydration products are ettringite and C-S-H gel[5, 6]. These products provide superior durability, making SSC highly resistant to sulfate and magnesite attack[7].

However, the compressive strength of SSC is highly sensitive to changes in the alkaline activator content[8], and its low early strength and inadequate long-termd strength limit its wide-spread use. Research has shown that the low early strength is mainly attributed to the

*Corresponding author **Kim Hung Mo,** *School of Engineering, Faculty of Engineering and Technology, Sunway University, No. 5, Jalan Universiti, Bandar Sunway, 47500, Selangor Darul Ehsan, Malaysia. Email: khmo@sunway.edu.my*
*Corresponding author **Pengkun Hou,** *School of Materials Science & Engineering, University of Jinan, Shandong, 250022, China. Email: pkhou@163.com*
Tongzhou Cai, *Department of Civil Engineering, Faculty of Engineering, Universiti Malaya, 50603 Kuala Lumpur, Malaysia. Email: 23103995@siswa.um.edu.my*
Heng Chen, *School of Materials Science & Engineering, University of Jinan, Shandong, 250022, China. Email: mse_chenh@ujn.edu.cn*

relatively slow dissolution rate of slag[9, 10], while the underdevelopment of late strength may be caused by the high concentration of calcium ion[11]. As a result, many researchers have explored various methods to improve the early and late strength of SSC.

As a critical component of SSC, the slag's alumina content[10, 12, 13] and dissolution rate significantly affect SSC's compressive strength. To improve the reaction rate of slag, many researchers have explored different approaches, such as high-temperature curing[14], increasing the fineness of slag[15], adding Na/K-lactate[16-18], or increasing the content of alkaline activator[10]. Moreover, slag dissolution requires a suitable alkaline environment. Zhai's[19] study shows that the optimal pH for slag hydration is 13.1. Additionally, the formation and precipitation of ettringite also require a suitable alkaline environment. Studies illustrate that ettringite cannot be present below pH 10.7[20]. Therefore, a proper alkaline environment is necessary to improve the compressive strength of SSC.

Numerous studies have illustrated that ultrafine nanoparticles enhance the dissolution and hydration of aluminosilicates such as cement, slag[21], and fly ash[22]. Nanosilica (NS) has been widely used in the study of performance modulation of cementitious materials because of its high pozzolanic reactivity and nucleation effect[23, 24]. Liu's[21] research revealed that 3 wt.% NS can effectively enhance the hydration and early compressive strength of slag in large dose slag systems. Li[11] found that the addition of 3 wt.% NS not only improves the early and late strength of SSC but also effectively regulates the pH of SSC and helps in reducing the concentration of calcium ion. Silica fume (SF)[25, 26], another highly reactive pozzolan, similarly regulates cementitious materials. SF supports the secondary hydration of C_3A[27], reduces porosity[28], enhances early strength and durability[29, 30], and diminishes the Ca/Si of C-S-H gel after hydration, reducing the risk of decalcification[31]. Existing studies focus either on NS or SF in SSC, but lack a systematic comparison of their effects under varying clinker content (e.g., 0.5-5 wt.%) and their interaction with hydration kinetics

This paper aims to compare and analyze the effects of adding 3 wt.% nanosilica and silica fume on the performance of each group of SSC with varying alkaline activator content. The objective is to provide a better understanding of the differences in the effects of these two siliceous materials on the performance of SSC.

2. Experimental

2.1 Raw materials

In this research, the main raw materials included slag, clinker, gypsum, silica fume (SF), and nanosilica (NS). The clinker was in accordance with the Chinese standard GB/T 21372-2008, and the physiochemical compositions of the clinker, slag, NS, and SF were measured by X-Ray Fluorescence (XRF) and are displayed in Table 1. The specific surface area of the clinker and GGBS was tested using the Blaine method, while the NS (with fumed hydrophilic properties) and SF were provided by the company, and the gypsum was purchased from Macklin, which was pure $CaSO_4 \cdot 2H_2O$. Additionally, the particle size distribution and scanning electron microscope (SEM) of all the raw materials was measured by laser diffraction, as shown in Fig. 1 and Fig. 2.

Table 1 Physiochemical properties of clinker, Slag, SF and NS (wt.%).

	CaO	SiO_2	Al_2O_3	SO_3	Fe_2O_3	MgO	LOI	SSA (m^2/kg)
Clinker	63.74	20.04	4.39	0.44	2.94	3.58	0.88	367
Slag	35.8	27.05	17.29	2.65	0.27	9.37	0.47	527
SF	0.124	96.643	0.214	0.046	0.311	-	1.09	273000
NS	-	≥98.0	-	-	-	-	-	300000

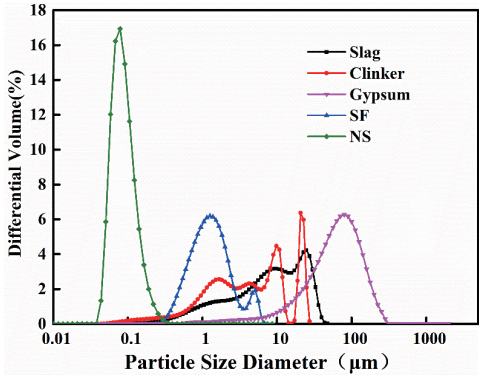

Fig. 1 The particle size distribution of all raw materials.

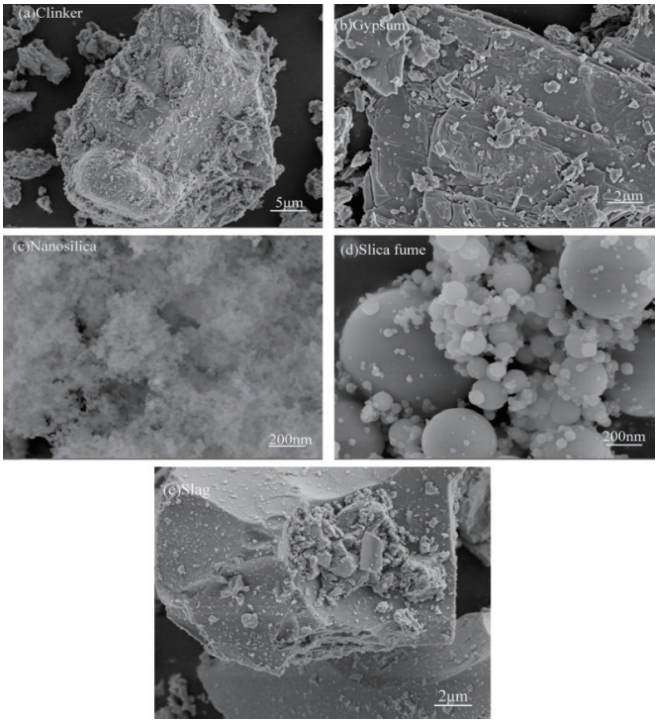

Fig. 2 The morphology images of (a) Clinker, (b) Gypsum, (c) Nanosilica, (d) Silica fume, (e) Slag.

2.2 Preparation of samples

Table 2 shows the mix proportions of the supersulfated cements (SSCs). Clinker was added at 0.5 wt.%, 1 wt.%, 3 wt.% and 5 wt.% (labeled as C0.5, C1, C3, and C5 as control groups). In addition, samples with 3% nanosilica (NS3) and 3% silica fume (SF3) were prepared as they showed the maximum performance in previous experiments[21, 32]. SF3 replaced part of GGBS. It is worth mentioning that NS and SF were dispersed in water via ultrasonic treatment (40 kHz, 30 min). The mortar's flow rate was adjusted to 170 mm using a polycarboxylate superplasticizer. The sand-to-binder ratio of 3.0 were used, which complied with the Chinese standard GB/T 17671-2021[33]. After molding, mortar samples were cured in standard curing chamber (22 ℃ and RH 95 %), demolded after setting and hardening, and then, continued curing to test the compressive strength of mortar at 3 d, 7 d, 28 d, and 90 d. The hydrated properties were tested using time-suited paste samples.

Table 2 Mix proportions of SSC pastes and mortars. (wt.%)

Samples	Clinker	Gypsum	Slag	NS	SF	Superplasticizer	
						Paste	Mortar
C0.5-SF3	0.5	15	82.5	0	3	1	2.5
C0.5-NS3	0.5	15	82.5	3	0	2.5	4.25
C1-SF3	1	15	81	0	3	1	2.5
C1-NS3	1	15	81	3	0	2.5	4.25
C3-SF3	3	15	79	0	3	1	2.5
C3-NS3	3	15	79	3	0	2.5	4.25
C5-SF3	5	15	77	0	3	1	2.5
C5-NS3	5	15	77	3	0	2.5	4.25

2.3 Experimental methods

2.3.1 mechanical property

The compressive strength of mortar samples was tested according to the Chinese standard GB/T 17671–2021[33].

2.3.2 hydration heat

The evolution of the heat of hydration of the samples was observed using an 8-channel isothermal heat calorimeter (TAM Air, TA Instruments Ltd., USA). The experimental environment was controlled at 25 °C, and an external stirring method was used to collect the early (3 d) hydration heat, which was more suitable for our system.

2.3.3 Thermogravimetric analysis (TG)

The thermal gravimetric analysis (TGA) data in this study was obtained using a TGA/DSC instrument (Mettler-Toledo) under argon gas. Approximately 20-30 mg of the sample was heated in an argon atmosphere at a rate of 10 ºC per minute from 30 ºC to 600 ºC. Prior to the testing, the sample was washed with ether, then placed in a vacuum drying oven to eliminate the influence of free water before 50 ºC.

2.3.4 Phase assemblage

The presence and content of hydration products were verified using X-ray diffraction. Corundum was used as an internal standard to determine the proportion of

each phase. Test samples were prepared by grinding 0.4 g of the sample and 0.1 g of α-Al_2O_3 with anhydrous ethanol for 30 minutes. The content of hydration phases was calculated using the TOPAS software.

2.3.5 Pore structure

Mercury intrusion porosimetry (MIP) testing was conducted using MicroActive AutoPore V 9600 to provide further insight into the pore structure evolution of SF/NS at 28 days for each alkalinity sample. The test samples weighed below 1 g, and the testing temperature was 24.65 . The contact angle was set at 130° and the test pore diameter range was approximately 3 nm to 350,000 nm. MIP testing helped to understand the pore structure of the samples in the later period.

2.3.6 Pore solution

The pore solution of 10 hours were obtain the paste samples, and the first 4 hours pore solution were centrifuged directly using 9000 rpm, while the last 6 hours were squeezed by concrete press machine (TYA-2000A). The obtained pore solution was tested for pH within 10 minutes (PHSJ-3F), followed by acidification with concentrated nitric acid to prevent precipitation of hydration products[9]. The acidified solution was diluted 10 times and 100 times, and the ion concentrations were measured (Perkin Elmer, Optima 3000). The saturation indices were calculated using GEMS software.

3. Results and discussion

3.1 Compressive strength

The compressive strength of SSC was investigated with the addition of 3 wt.% nanosilica (NS) and silica fume (SF) at 0.5 wt.%, 1 wt.%, 3 wt.%, and 5 wt.% cement clinker and testing dates, as shown in Fig. 3. The growth of compressive strength ratio after NS and SF addition is presented in Fig. 4.

The results demonstrate that the addition of NS and SF has similar positive influences on the compressive strength of 3 days with increasing clinker (Fig. 3), which is unaffected by variations in Si properties. The SF-added samples reached peak strength at C1 after 7 days, which progressively developed until 90 days, although it was lower than the blank in the early stages (before 7 d). The C1-NS3 sample showed similar behavior in later stages, although its 7-day compressive strength was lower in C3 and C5 samples, consistent with previous research[8]. Furthermore, both SF and NS effectively enhanced the strength of C3 and C5 samples from early to late stages (Fig. 4), which differed from C0.5 and C1, with more pronounced effects at later ages of C3. The C3 added-NS samples demonstrated nearly the same late strength as the C1-added samples (i.e., a decline from 12 MPa to 2.62 MPa at 90 days). However, SF did not have a significant effect in this range. The 3 wt.% NS could reduce sensitivity between C1 and C3, consistent with previous findings[8]. The results indicated that the most suitable clinker dosage range in the SSC system is between 1 wt.% and 3 wt.%, where 3 wt.% SF and NS could play a key role in early and later hydration times. The dosage of NS did not affect this outcome and could decrease the clinker sensitivity.

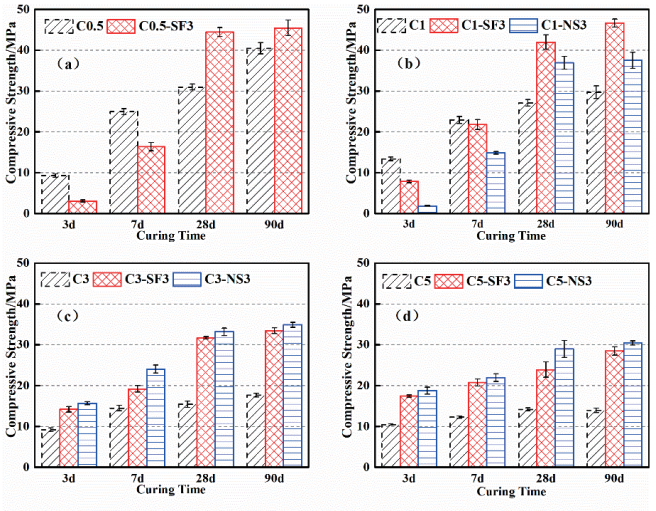

Fig. 3 Compressive strength development of SSC with NS and SF addition under different clinker contents.

Fig. 4 shows that SF and NS had similar compressive strength enhancement effects on all samples in later periods (28 and 90 days). SF significantly increased the strength of C1 and C3 samples at 28 and 90 days (55.01% and 57.14% for C1 sample; 105.38% and 89.47% for C3 sample, respectively). Similarly, NS

also significantly increased the strength of C1 and C3 samples at 28 and 90 days (36.31% and 26.26% for C1 sample; 114.98% and 97.78% for C3 sample, respectively). SF and NS also showed significant differences in the C1 and C3 groups. The compressive strength of SF was better than NS in the C1 group, while NS performed better than SF and the blank in the C3 samples. Additionally, the C0.5-NS3 sample showed no compressive strength as it could not harden during the experiment until 90 days. This could be due to unsuitable internal hydration reaction conditions for forming hydration products (ettringite and C-S-H gel), which will be explained in detail in the discussion section. The significant difference in the effect of SF and NS on the clinker groups of SSC has not been studied previously.

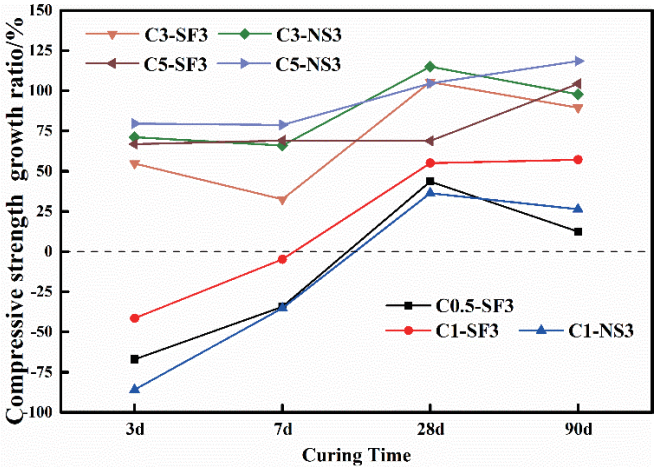

Fig. 4 The comparison of the effect of NS and SF on the compressive strength growth ratio of SSC.

The influence of SF and NS on the strength of SSC varies with clinker content and age. This can be attributed to the inhibitory effect of SF and NS on the hydration of the aluminate phase[27, 34], which affects the formation of ettringite - considered the primary performance in the early stages of SSC. However, SF and NS can enhance the hydration of the silica phase, leading to the growth of C-S-H gel, which is the main source of late compressive strength in SSC. Additionally, the difference in particle size and pozzolanic activity between NS and SF can also contribute to the unutilized effect on calcium ion adsorption[11].

Furthermore, the distinct trends of compressive strength at early and later ages observed with the addition of SF and NS imply different mechanisms of influence of SF and NS on the hydration and hardening process of the alkali-activated SSC system. These mechanisms are discussed in the following sections.

3.2 Heat of hydration

The impact of NS and SF on the early period (3 days) hydration of SSC was investigated through the measurement of hydration heat flow rate and total heat, and the results are presented in Fig. 5.

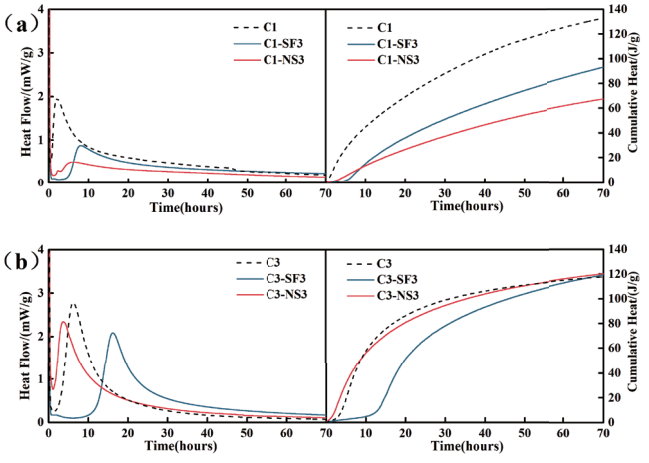

Fig. 5 The comparison of the effect of NS and SF on the hydration heat of C1 and C3.

During the early period, all samples exhibited a wide peak resulting from the dissolution of GGBS and the formation of ettringite[35] as a result of the reaction between aluminate and gypsum phases. However, the addition of NS and SF led to substantial changes in the hydration heat characteristics for all samples.

The addition of NS and SF exerted significantly different effects on C1/C3. In the C1 sample, the cumulative heat of hydration was inhibited and halved, and the exothermic hydration peak shifted to the right after the inclusion of NS and SF. Notably, NS exerted a stronger inhibitory effect than SF in C1 samples, consistent with their 3-day compressive strength (Fig. 3). In contrast, NS and SF showed utterly different trends in the C3 group compared to the C1 sample. The addition of NS resulted in a leftward shift of

the heat flow peak, while SF shifted significantly in the opposite direction. Moreover, NS yielded higher cumulative heat than SF aligning with prior studies[36]. The impact of SF was not as pronounced as NS in the C3 sample, which may be attributed to the different activity of silica fume and nanosilica. Importantly, the heat hydration of the C3 samples was consistent with compressive strength development (Fig. 3.).

Additionally, it is important to note that the cumulative heat release after the addition of NS and SF exhibited significant differences in both the C1 and C3 samples. The variation in heat release can be attributed to the degree of reactivity between NS and SF, as well as differences in their ability to form hydration products (ettringite and C-S-H gel). These factors will be further discussed in the following sections.

3.3 Hydration products

The results of TGA (Thermal Gravimetric Analysis) analyses for blank-, NS-, and SF-group samples at 3 days and 28 days are depicted in Fig. 6. Comparison of the curves in Fig. 6 with reference substances' data indicates the presence of ettringite, gypsum, and C-S-H gel. Furthermore, the XRD pattern in Fig. 7 identifies the presence of ettringite and gypsum. Notably, the addition of SF and NS did not alter the primary crystal hydration products of SSC.

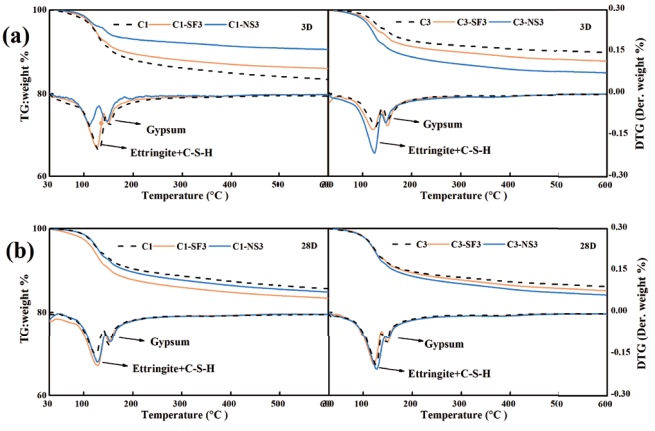

Fig. 6 TG and DTG date of C1 and C3 at 3 d and 28 d.

Fig. 6 shows that the addition of SF and NS led to a decrease in the formation of ettringite (shorter peak of ettringite and C-S-H) at 3 days. Moreover, the peak height of ettringite and C-S-H was more significant in the SF and NS added samples compared to the non-added samples at 28 days. The inhibitory effect of NS was stronger than that of SF in the C1 group.

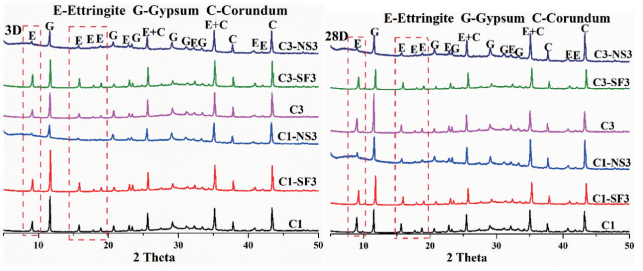

Fig. 7 XRD patterns of C1 and C3.

In contrast, the results showed an opposite trend in the C3 sample, where SF and NS promoted the growth of hydrates (higher peak of ettringite and C-S-H) until 28 days. Moreover, the effect of SF was better than that of NS. This phenomenon was consistent with the QXRD results in Tables 3 and 4 and the trend of transformation in the hydrates' peak and bound water content, as demonstrated in the compressive strength results (Fig. 3).

Table 3 Effects of NS and SF on the hydration products phase of C1.

SSC	Phase	Sample ID	3 d	28 d
C1	Gypsum	Blank	4	2.99
		SF3	3.07	2.61
		NS3	7.31	5.05
	Ettringite	Blank	8.32	12.46
		SF3	9.53	11
		NS3	6.02	7.43
	Amorphous phase	Blank	84.69	81.66
		SF3	83.98	83.33
		NS3	83.65	82.67

Table 4 Effects of NS and SF on the hydration products phase of C3.

SSC	Phase	Sample ID	3 d	28 d
C3	Gypsum	Blank	5.23	3.44
		SF3	2.35	2.08
		NS3	6.13	7.04
	Ettringite	Blank	8	12.11
		SF3	10.6	10.97
		NS3	7.1	6.46
	Amorphous phase	Blank	84.03	81.58
		SF3	84.04	84.18
		NS3	81.27	81.8

NS addition decreased ettringite content by reducing gypsum consumption across all samples and ages, while promoting amorphous phase (C-S-H gel) formation, according to the results presented in Tables 3 and 4. This phenomenon was also observed by others[34] and was attributed to the electrostatic adsorption effect, leading to a reduction in hydration production. On the other hand, a slight reduction in gypsum and an increase in ettringite in the SF-added samples were observed at 3 days, but the ettringite content decreased later. This can be attributed to SF inhibiting C_3A hydration later than NS. SF's larger particle size may delay its suppression of ettringite formation. Moreover, both SF and NS were suitable for forming an amorphous phase at 28 days, which may explain the early reduction and later improvement in compressive strength observed in the C1 group (Fig. 3).

There were significant differences in the reaction of SF and NS in the C1/C3 groups of SSC. This can be attributed to the difference in activity between the SF and NS, but more importantly, the difference in the influence of ions and pH value, which led to variations in the hydration products.

3.4 Microstructure

The Mercury intrusion porosimetry (MIP) technique was investigated the impact of SF and NS on the pore structure of SSC at 28 d (Fig. 8), which covers the pore size range from approximately 5 nm to 1000 nm.

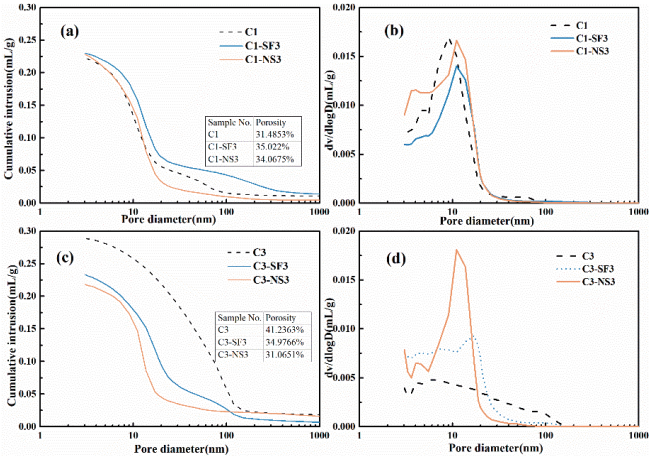

Fig. 8 Pore analysis of C1 and C3 at 28d.

At C3 sample, it was observed that the addition of SF and NS resulted in a lower porosity compared to the non-added sample, indicating that SF and NS could densify the microstructure and enhance the compressive strength development at 28 days as illustrated in Fig. 3. Furthermore, the addition of SF and NS caused the most probable pore diameters to gradually decrease. The leftward shift of cumulative intrusion curves (Figs. 8a, 8c) indicates pore structure refinement. Thus, the incorporation of SF and NS validates the mechanism that significantly densified the microstructure of the C3 sample due to filling and pozzolanic effects[23, 37]. However, the porosity of the NS-added sample is lower than that of the SF-added sample, which could be attributed to the superior pozzolanic effects of NS compared to SF, and the smaller size of NS.

Pore size distribution curves for SF/NS-modified C1 and C3 samples are shown in Figs. 8b and 8d. The samples were divided into five categories based on their pore sizes: gel micro-pores (<20 nm), meso-pores (20–50 nm), middle capillary pores (50–100 nm), large capillary pores (100–5000 nm), and macro-pores (>5000 nm)[37, 38]; the pore volume fraction within each range was shown in Fig. 9. The results in Fig. 9b demonstrate that the added SF and NS samples of C3 had more gel pores and fewer middle capillary and macro-pores. Furthermore, the added-NS samples had more gel pores than the added-SF samples. It has been reported that gel micro-pores correspond to gel pores in C-S-H[39]. This suggests that the use of NS can lead to a denser compressive strength due to the filling effect of the C-S-H gel produced by the high pozzolanic nature of NS itself.

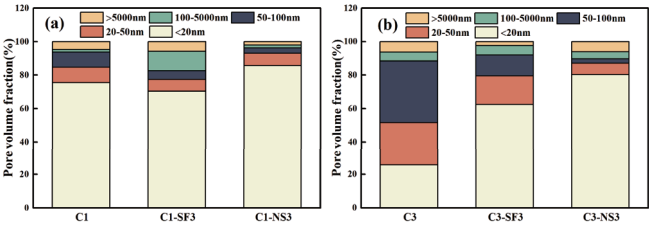

Fig. 9 Pore volume fraction of C1 and C3.

3.5 Pore solution analysis

To understand the underlying cause of the failure

of C0.5-NS3 to fully hydrate and harden, the concentration of ions, saturation index, and pH values in the pore solution within the first 10 hours were analyzed. The results are presented in Fig. 10-12.

Fig. 10 reveals the presence of S^{2-}, Ca^{2+}, Si^{4+}, and Al^{3+} ions in the pore solutions. As hydration progressed, the amount of Si^{4+} and S^{2-} ions decreased in the added SF samples compared to the blank sample, while the concentrations of Ca^{2+} and Al^{3+} ions increased due to the precipitation of hydrates. It was also observed that the Ca^{2+} ion concentration increased in the NS-added sample relative to the blank sample, which may be attributed to the adsorption with NS.

However, the change in Si ion concentration was different from the expected trend, as the addition of SF and NS was expected to increase the concentration of Si^{4+}, and the formation of C-S-H gel would consume more Si^{4+} ion. However, the Si^{4+} concentration in the NS-added sample showed an increasing trend compared to the blank and SF-added samples, and it was over 3 mmol/L. This suggested that Si^{4+} from NS did not participate in the process shown in Fig. 10a. Moreover, the S and Al ion concentrations in the NS-added sample remained constant within the first 10 hours, while the blank and SF-added samples varied during the same time period. This observation indicates that no hydration products were formed in the NS-added sample of C0.5, which could affect the concentration of the pore solution. The saturation index data further corroborated this result, as the hydrates in the NS-added group were always in an undersaturated state, as shown in Fig. 11, whereas the blank and SF-added groups showed the opposite trend within the first 10 hours.

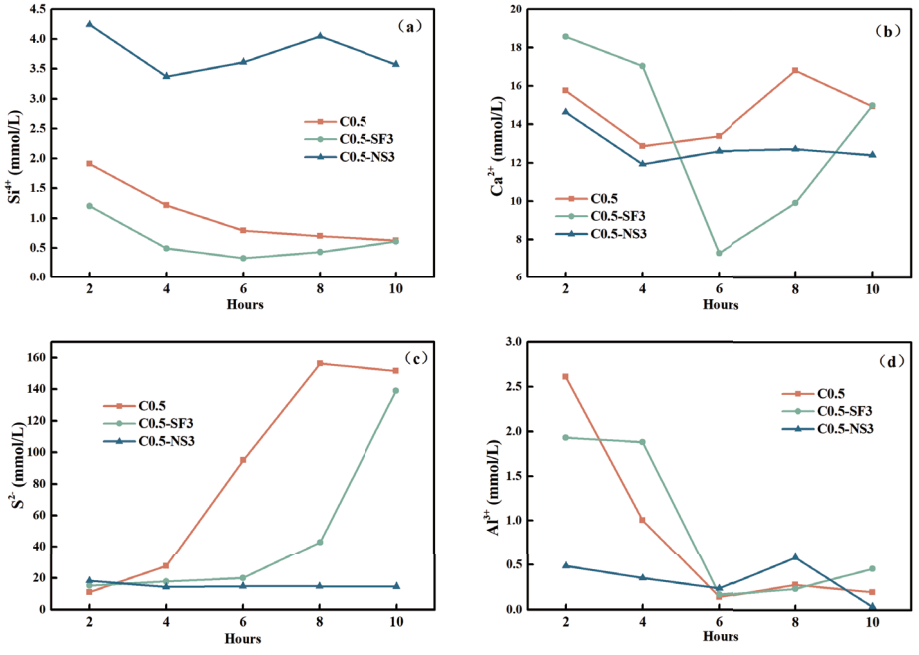

Fig. 10 Effect of NS and SF on the concentration of each ion in the pore solution.

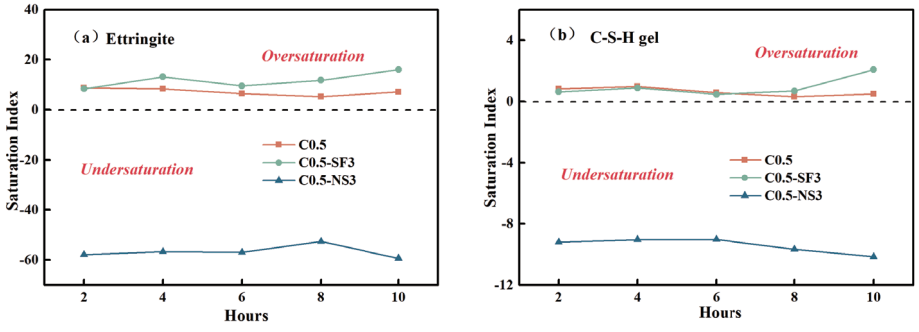

Fig. 11 Effect of NS and SF on the saturation index of hydration products.

Additionally, adding SF maintained a comparable pH value with the blank sample, while NS lowered the pH from 12.2 to nearly 10.1. The pH level remained relatively constant during the first 10 hours, as shown in Fig. 12. The dissolution of the slag required a high pH value[19], and the hydration growth condition of ettringite was higher than a pH of 10.7[20]. This is likely the reason why the compressive strength of C0.5-NS3 did not improve until the 90-day mark.

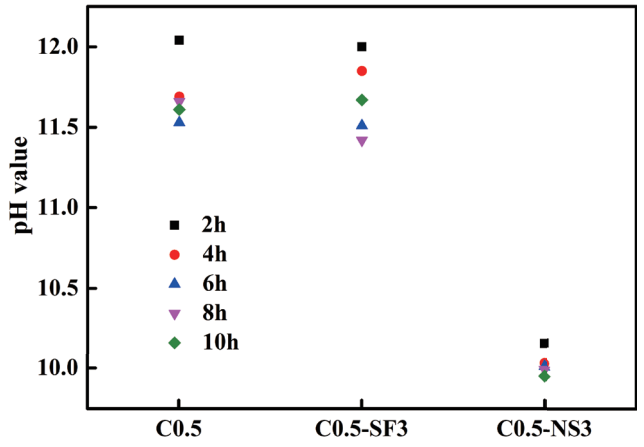

Fig. 12 Effect of NS and SF on the early pH value of C0.5.

4. Conclusion

In this study, the effects of NS and SF on the properties of supersulfated cement were compared and analyzed through mechanical performance, hydration product evolution, microstructure characteristics, and ions reactions. Based on the experimental results obtained, the following conclusions can be drawn:

a: Both NS and SF improved the mechanical properties of supersulfated cement in the later period. However, the enhancing effect of NS was consistently greater than that of SF in the higher-clinker group. In contrast, SF was more effective than NS in the lower-clinker group, and C0.5-NS3 sample never achieved compressive strength, which is related to the difference in their ability to consume calcium ions and NS's significant pH reduction may hinder slag activation in low-clinker SSC.

b:Both NS and SF effectively reduce early hydration heat evolution in C1, though their impacts on C3 are less pronounced. In C3 samples, NS accelerates hydration, whereas SF delays it. These differences may be attributed to their varying effects on ettringite and amorphous substances. NS demonstrates a greater ability to reduce ettringite content and inhibit gypsum consumption compared to SF. However, both materials promote the formation of amorphous substances. The distinct particle sizes and pozzolanic reactivity of NS and SF play a crucial role in these outcomes, with SF's micro-sized particles leading to a delayed suppression effect on ettringite.

c: The NS group had a lower porosity and a higher content of gel pores compared with the SF group, which may be related to its higher pozzolanic activity and particle sizes.

d: NS effectively reduced pH and saturation index, unlike SF, which showed no significant effect. This variation is attributed to their differing capacities to consume calcium ions. Consequently, SF is appropriate for low-clinker systems such as eco-pavements, whereas NS is better suited for high-clinker structural elements requiring sustained strength over time.

CRediT authorship contribution statement:

Tongzhou Cai: Methodology, Writing - original draft, Writing - review & editing. Kim Hung Mo: Methodology, Supervision, Writing - original draft, Writing - review & editing. Heng Chen: Methodology, Writing - original draft, Writing - review & editing. Pengkun Hou: Conceptualization, Methodology, Supervision, Writing - original draft, Writing - review & editing.

Declaration of competing interest:

The authors declare that they have no known competing financial interests or personal relationships that could have appeared to influence the work reported in this paper.

Acknowledgements:

The authors gratefully acknowledge supports from National Key R&D Program (2023YFE0126000). This project has also received support from the 111 Project of International Corporation on Advanced

Cement-based Materials (No. D17001), which is also acknowledged.

Reference

[1] J, Wei.; K, Cen.; and Y, Geng. (2019) "Evaluation and mitigation of cement CO2 emissions: projection of emission scenarios toward 2030 in China and proposal of the roadmap to a low-carbon world by 2050," Mitigation and Adaptation Strategies for Global Change, 24(2), pp. 301~328.

[2] Q, Wu.; Q, Xue.; and Z, Yu. (2021) "Research status of super sulfate cement, " Journal of Cleaner Production, 294, pp. 126228.

[3] S, Liu.; L, Wang.; and B, Yu. (2019) "Effect of modified phosphogypsum on the hydration properties of the phosphogypsum-based supersulfated cement," Construction and Building Materials, 214, pp. 9~16.

[4] K, Cabrera-Luna.; E,E, Maldonado-Bandala.; D, Nieves-Mendoza.; and J,I, Escalante García. (2018) "Supersulfated binders based on volcanic raw material: Optimization, microstructure and reaction products," Construction and Building Materials, 176, pp. 145~155.

[5] H, Yazıcı.; M,Y, Yardımcı.; H, Yiğiter.; S, Aydın.; and S, Türkel. (2010) "Mechanical properties of reactive powder concrete containing high volumes of ground granulated blast furnace slag," Cement and Concrete Composites, 32(8) , pp. 639~648.

[6] S,A, Bernal.; J,L, Provis.; V, Rose.; and R, Mejía de Gutierrez. (2011) " Evolution of binder structure in sodium silicate-activated slag-metakaolin blends," Cement and Concrete Composites, 33(1) , pp. 46~54.

[7] S,R, Pinto.; C, Angulski da Luz.; G,S, Munhoz.; and R,A, Medeiros-Junior. (2020) "Durability of phosphogypsum-based supersulfated cement mortar against external attack by sodium and magnesium sulfate," Cement and Concrete Research, 136, pp. 106172.

[8] T, Cai.; P, Hou.; H, Chen.; P, Zhao.; P, Du.; S, Wang.; X, Zhou.; X, Wang.; and X, Cheng. (2023) "Effects of nanosilica on supersulfated cements of different clinker-activation degree," Construction and Building Materials, 365, pp. 130118.

[9] A, Gruskovnjak.; B, Lothenbach.; F, Winnefeld.; R, Figi.; S,C, Ko.; M, Adler.; and U, Mäder. (2008) "Hydration mechanisms of super sulphated slag cement," Cement and Concrete Research, 38(7), pp. 983~992.

[10] R, D, Hooton.; and R, Masoudi.; (2019) "Examining the hydration mechanism of supersulfated cements made with high and low-alumina slags," Cement and Concrete Composites, 103 pp. 193~203.

[11] B, Li.; P, Hou.; H, Chen.; P, Zhao.; P, Du.; S, Wang.; and X, Cheng. (2022) "GGBS hydration acceleration evidence in supersulfated cement by nanoSiO2", Cement and Concrete Composites, 132, pp. 104609.

[12] T, Matschei. (2005) "Hydration behaviour of sulphate-activated slag cements," Advances in Cement Research, 17(4), pp. 167–178.

[13] M, Whittaker.; M, Zajac.; M, Ben Haha.; F, Bullerjahn.; and L, Black. (2014) "The role of the alumina content of slag, plus the presence of additional sulfate on the hydration and microstructure of Portland cement-slag blends," Cement and Concrete Research, 66, pp. 91~101.

[14] C, Angulski da Luz.; and R, D, Hooton. (2015) "Influence of curing temperature on the process of hydration of supersulfated cements at early age," Cement and Concrete Research, 77, pp. 69~75.

[15] S, Liu.; L, Wang.; Y, Gao.; B, Yu.; and W, Tang. (2015) "Influence of fineness on hydration kinetics of supersulfated cement," Thermochimica Acta, 605, pp. 37~42.

[16] R, Masoudi.; and R, D, Hooton. (2020) "Influence of alkali lactates on hydration of supersulfated cement," Construction and Building Materials, 239, pp. 117844.

[17] Y, Zhou.; Z, Peng.; L, Chen.; J, Huang.; and T, Ma. (2021) "The influence of two types of alkali activators on the microstructure and performance of supersulfated cement concrete mitigating the strength and carbonation

resistance," Cement and Concrete Composites, 118, pp. 103947.

[18] Z, Peng.; Y, Zhou.; J, Wang.; L, Chen.; and C, Miao. (2022) "The impediment and promotion effects and mechanisms of lactates on the hydration of supersulfated cements - Aiming at a performance enhancement," Journal of Cleaner Production, 341, pp. 130751.

[19] Q, Zhai.; and K, Kurumisawa. (2022) "Effects of cation in sulfate chloride and nitrite on Ca(OH)2 activated ground granulated blast-furnace slag," Cement and Concrete Composites, 133, pp. 104648.

[20] E,A, Kishar. (2005) "Hydration reaction of tricalciumaluminate in different systems," Cement and Concrete Research, 35(8), pp. 1638-1640.

[21] X, Liu.; P, Hou.; and H, Chen. (2021) "Effects of nanosilica on the hydration and hardening properties of slag cement," Construction and Building Materials, 282, pp. 122705.

[22] P, Hou.; S, Kawashima.; K, Wang.; D, J, Corr.; J, Qian.; and S,P, Shah. (2013) "Effects of colloidal nanosilica on rheological and mechanical properties of fly ash–cement mortar," Cement and Concrete Composites, 35(1), pp.12~22.

[23] S, Kawashima.; P, Hou.; D, J, Corr.; and S, P, Shah. (2013) "Modification of cement-based materials with nanoparticles," Cement and Concrete Composites, 36, pp. 8~15.

[24] P, Hou.; S, Kawashima.; D, Kong.; D, J, Corr.; J, Qian.; and S, P, Shah. (2013) "Modification effects of colloidal nanoSiO2 on cement hydration and its gel property," Composites Part B: Engineering, 45(1), pp. 440~448.

[25] B, Uzal.; L, Turanlı.; H, Yücel.; M, C, Göncüoğlu.; and A, Çulfaz. (2010) "Pozzolanic activity of clinoptilolite: A comparative study with silica fume, fly ash and a non-zeolitic natural pozzolan," Cement and Concrete Research, 40(3), pp. 398~404.

[26] H, Wang.; X, Liu.; and Z, Zhang. (2023) "Pozzolanic activity evaluation methods of solid waste: A review," Journal of Cleaner Production, 402, pp. 136783.

[27] X, Wang.; P, Hou.; J, Yu.; X, Zhou.; and X, Cheng. (2020) "The effects of silica fume on C3A hydration," Construction and Building Materials, 250, pp. 118766.

[28] Y, Zhang.; J, Chang.; Q, Zhao.; W, L, Lam.; P, Shen.; Y, Sun.; D, Zhao.; and C,S, Poon. (2022) "Effect of dosage of silica fume on the macro-performance and micro/nanostructure of seawater Portland cement pastes prepared with an ultra-low water-to-binder ratio," Cement and Concrete Composites, 133, pp. 104700.

[29] K, Yuan.; W, Ni.; L, Zhao.; and H, Wang. (2023) "Silica fume stabilized loess: Mechanical properties, microstructural evolution and environmental analysis," Sustainable Materials and Technologies, 36, pp. e00604.

[30] W, Xu.; Y, Zhang.; X, Zuo.; and M, Hong. (2020) "Time-dependent rheological and mechanical properties of silica fume modified cemented tailings backfill in low temperature environment," Cement and Concrete Composites, 114, pp. 103804.

[31] W, Kunther.; B, Lothenbach.; and J, Skibsted. (2015) "Influence of the Ca/Si ratio of the C–S–H phase on the interaction with sulfate ions and its impact on the ettringite crystallization pressure," Cement and Concrete Research, 69, pp. 37~49.

[32] Z, Wu.; C, Shi.; and K, H, Khayat. (2016) "Influence of silica fume content on microstructure development and bond to steel fiber in ultra-high strength cement-based materials (UHSC)," Cement and Concrete Composites, 71, pp. 97~109.

[33] Method of testing cememts-determination of strength,GB/T17671-2021.

[34] P, Hou.; X, Wang.; P, Zhao.; K, Wang.; S, Kawashima.; Q, Li.; N, Xie.; X, Cheng.; and S, P, Shah. (2020) "Physicochemical effects of nanosilica on C3A/C3S hydration," Journal of the American Ceramic Society, 103(11), pp. 6505~6518.

[35] H, Minard.; S, Garrault.; L, Regnaud.; and A, Nonat. (2007) "Mechanisms and parameters controlling the tricalcium aluminate reactivity in the presence of gypsum," Cement and Concrete

Research, 37(10), pp. 1418~1426.
[36] H, Yang.; M, Monasterio.; D, Zheng.; H, Cui.; W, Tang.; X, Bao.; and X, Chen. (2021) "Effects of nano silica on the properties of cement-based materials: A comprehensive review," Construction and Building Materials, 282, pp. 122715.
[37] Z, Xu.; J, Gao.; Y, Zhao.; S, Li.; Z, Guo.; X, Luo.; and G, Chen. (2022) "Promoting utilization rate of ground granulated blast furnace slag (GGBS): Incorporation of nanosilica to improve the properties of blended cement containing high volume GGBS," Journal of Cleaner Production, 332, pp. 130096.
[38] Z, Wu.; K, H, Khayat.; and C, Shi. (2017) "Effect of nano-SiO2 particles and curing time on development of fiber-matrix bond properties and microstructure of ultra-high strength concrete," Cement and Concrete Research, 95, pp. 247~256.
[39] H, M, Jennings. (2000) "A model for the microstructure of calcium silicate hydrate in cement paste," Cement and Concrete Research, 30(1), pp. 101-116.